Original Article

MOLECULAR METABOLISM

PPARγ is dispensable for clear cell renal cell carcinoma progression

Danielle J. Sanchez [1,4], David J. Steger [3], Nicolas Skuli [1,2], Ankita Bansal [1,2], M. Celeste Simon [1,4,*]

ABSTRACT

Objective: Clear cell renal cell carcinoma (ccRCC) is a subtype of kidney cancer defined by robust lipid accumulation, which prior studies have indicated plays an important role in tumor progression. We hypothesized that the peroxisome proliferator-activated receptor gamma (PPARγ), detected in both ccRCC tumors and cell lines, promotes lipid storage in ccRCC and contributes to tumorigenesis in this setting. PPARγ transcriptionally regulates a number of genes involved in lipid and glucose metabolism in adipocytes, yet its role in ccRCC has not been described. The objective of this study was to elucidate endogenous PPARγ function in ccRCC cells.

Methods and results: Using chromatin immunoprecipitation followed by deep sequencing (ChIP-seq), we found that PPARγ and its heterodimer RXR occupy the canonical DR1 PPAR binding motif at approximately 1000 locations throughout the genome that can be subdivided into adipose-shared and ccRCC-specific sites. CRISPR-Cas9 mediated, loss-of-function studies determined that PPARγ is dispensable for viability, proliferation, and migration of ccRCC cells *in vitro* and *in vivo*. Also, surprisingly, PPARγ deletion had little effect on the robust lipid accumulation that typifies the "clear cell" phenotype of kidney cancer.

Conclusion: Our results suggest that PPARγ plays neither a tumor suppressive nor oncogenic role in advanced ccRCC, and thus single-agent therapeutics targeting PPARγ are unlikely to be effective for the treatment of this disease. The unique cistrome of PPARγ in ccRCC cells demonstrates the importance of cell type in determining the functions of PPARγ.

Keywords Nuclear receptors; PPARγ; Kidney cancer; Cancer metabolism; Lipid metabolism

1. INTRODUCTION

Kidney cancer is the 8th most prevalent form of cancer diagnosed each year in the United States, with approximately 64,000 new diagnoses and 14,400 deaths annually [1]. While localized disease can be treated by surgical resection, 30% of patients initially present in the clinic with metastatic disease, which carries a poor prognosis due to limited efficacy of current standard-of-care therapies [2]. As such, a significant clinical need remains for therapeutics targeting unique genetic and metabolic vulnerabilities within this tumor type.

Clear cell renal cell carcinoma (ccRCC), the most common subtype of kidney cancer, is defined by constitutive hypoxia-inducible factor signaling as well as widespread changes in cellular metabolism of glucose, amino acids, and lipids [3]. Phenotypically, ccRCC is characterized by robust intracellular lipid and glycogen accumulation, resulting in "cleared" cytoplasm when prepared for common histologic analyses. Rather than simply reflecting a byproduct of increased anabolic metabolism, recent studies suggest that maintaining the integrity of neutral lipid droplets as well as abundant lipid uptake is critical to maintain ccRCC cell viability [4], particularly when oxygen is limiting in the tumor microenvironment [5]. However, factors imparting a lipogenic quality to ccRCC tumors remain to be fully elucidated.

The peroxisome proliferator-activated receptor gamma (PPARγ) along with its heterodimeric DNA-binding partner retinoid X receptor (RXR) promote the transcription of genes broadly important for lipid, glucose, and hormone metabolism, most notably in the context of adipose tissue [6]. PPARγ, the master regulator of adipogenesis, is both necessary and sufficient for this process *in vitro* and *in vivo* [7] [8]. Additionally, in non-adipose contexts including ischemic, diseased cardiomyocytes [9] and macrophages [10], PPARγ contributes to the regulation of genes involved in lipid metabolism. In a mouse model of high fat diet (HFD)-induced hepatosteatosis, PPARγ protein expression is elevated in the livers of mice fed HFD relative to controls [11], although the absolute level remains far below those observed in adipose tissues. Interestingly, conditional deletion of *Pparg* within hepatocytes abrogated liver steatosis, suggesting a link between PPARγ and lipid uptake, synthesis, and/or storage in this model.

Previous reports indicate that PPARγ is functionally expressed [12] in ccRCC and that increased PPARγ abundance correlates with reduced patient survival [13], suggesting a possible oncogenic function. *In vitro* studies investigating the role of PPARγ in ccRCC and other cancers have largely employed natural and synthetic activating ligands including the insulin-sensitizing thiazolidinediones, yet many used super-physiologic concentrations, which can cause off-target effects

[1]Abramson Family Cancer Research Institute, USA [2]Department of Cancer Biology, USA [3]Institute for Diabetes, Obesity and Metabolism, USA [4]Department of Cell and Developmental Biology, USA

*Corresponding author. Perelman School of Medicine at the University of Pennsylvania, 456 BRB II/III, 421 Curie Boulevard, Philadelphia, PA, 19104-6160, USA. E-mail: celeste2@pennmedicine.upenn.edu (M.C. Simon).

Received May 1, 2018 • Revision received May 11, 2018 • Accepted May 17, 2018 • Available online 21 May 2018

https://doi.org/10.1016/j.molmet.2018.05.013

and confound interpretation of results [14,15]. In this study, our goal was to investigate endogenous PPARγ function through ChIP-seq and a number of *in vitro* and *in vivo* assays of tumor progression using loss-of-function models in established ccRCC cell lines.

2. MATERIALS AND METHODS

2.1. Primary patient samples and gene expression data

Matched tumor/normal samples were obtained from the Cooperative Human Tissue Network (CHTN). Tumors were homogenized in TRIzol (see quantitative real-time PCR) or whole cell elution buffer (see western blot) and analyzed for *PPARG* mRNA and protein expression. Gumz et al. microarray dataset was downloaded from Oncomine. RNA-seq data for 480 ccRCC and 69 normal kidney samples were downloaded from TCGA on April 2, 2013. Differential gene expression analysis of tumor and normal samples was performed using DeSeq (Bioconductor Version 2.12). TCGA mutation and copy number data for 418 sequenced patients/cases were downloaded from cBioPortal for Cancer Genomics [16].

2.2. Cell culture, plasmids, lentiviral production, and viral transduction

Human ccRCC cell lines (RCC10, UMRC2, Caki2, 786-O, A498, 769-P) were obtained from the American Type Culture Collection (ATCC) and were cultured in DMEM (ThermoFisher Scientific, cat. 11965092) supplemented with 10% FBS (Gemini Bio-Products, cat. 900-108). Immortalized renal epithelial cells (HK2) obtained from ATCC and cultured in Keratinocyte Serum Free Media with appropriate supplements (ThermoFisher Scientific, cat. 17005042). Human single-guide RNAs (sgRNA) targeting *PPARG* #1 (ctccgtggatctctccgtaa) and #3 (cattacgaagacattccatt) along with control gRNA targeting mouse *Rosa26* locus (aagatgggcgggagtcttct) were cloned into LentiCRISPRv2 plasmid [17]. Mature antisense human *PPARG* shRNA #3 sequence (clone ID: TRCN0000001673) along with scrambled (SCR) control were cloned into a doxycycline-inducible pLKO lentiviral plasmid (AddGene, cat. 21915, [18]). Lentivirus was prepared by co-transfection of 293T cells with shRNA or CRISPR plasmid of interest along with packaging plasmids pVSVg (AddGene, cat. 8454), psPAX2 (AddGene, cat. 12260) and Fugene6 transfection reagent (Promega). Lentivirus-containing media was collected from plates at 24 and 48 h post-transfection, filtered using a 0.45 μm filter, and stored at −80 °C. For viral transduction, cells were incubated with lentivirus-containing medium and 8 μg/mL polybrene for 24 h. Cells were allowed to recover for another 24 h before selection with puromycin. All experiments were performed with cells that survived puromycin selection and displayed knockdown/knockout of *PPARG* as assayed by western blot.

2.3. Quantitative real-time PCR (qRT-PCR)

Total RNA was isolated using TRIzol reagent (ThermoFisher Scientific, cat. 15596026) and RNeasy mini kit (Qiagen, cat. 74104). Reverse transcription was performed using High-Capacity RNA-to-cDNA (Applied Biosystems, cat. 4387406). qRT-PCR was performed using ViiA7 Real-Time PCR system (Applied Biosystems) with TaqMan master mix (Life Technologies). TaqMan probes were used to quantitate expression of *PPARG* (cat. Hs01115513_m1), *FABP4* (cat. Hs01086177_m1), *CD36* (cat. Hs01567185_m1) *SLC38A4* (Hs00394339_m1) and normalized to housekeeping genes *HPRT1* (cat. Hs02800695_m1) and *TBP* (Hs00427620_m1).

2.4. Western blot

Cells were washed with PBS prior to lysis in whole cell elution buffer (150 mM NaCl, 10 mM Tris pH 7.6, 0.1% SDS, and 5 mM EDTA) containing Roche ULTRA protease inhibitor cocktail (cat. 05892791001). Proteins were resolved by SDS-PAGE, transferred to nitrocellulose membranes, and immunoblotting was performed by incubating with primary antibodies overnight at 4 °C. The next day, membranes were incubated with secondary antibody and Western Lightning Plus-ECL, Enhanced Chemiluminescence Substrate (PerkinElmer, cat. NEL103E001EA) was used to visualize proteins. All primary antibodies were diluted of 1:1000 in 5% w/v nonfat milk (except GAPDH, 1:10,000), and secondary antibodies were diluted 1:2000 in 5% w/v nonfat milk. PPARγ (cat. 2435), FASN (cat. 3180), GAPDH (cat. 2118), anti-Rabbit IgG, HRP-linked (cat. 7074), anti-Mouse IgG, HRP-linked (cat. 7076) were purchased from Cell Signaling Technology. SREBP1 (cat. 13551) was purchased from Santa Cruz Biotechnology. SCD (cat. 19862) was purchased from Abcam.

2.5. Chromatin immunoprecipitation (ChIP) and ChIP-seq

ChIP was performed with whole cell extracts isolated from UMRC2 PPARγ WT and PPARγ KD cell lines using 10 μg PPARγ (Santa Cruz, cat. sc-7196) or 10 μg RXRα/β/γ (Santa Cruz, cat. sc-774) antibodies for immunoprecipitation (IP). Briefly, confluent 10 cm dishes of cells were prepared by crosslinking with 1% formaldehyde for 15 min at room temperature and quenched with 125 mM glycine for 5 min at room temperature. Cells were harvested by scraping and pellets were resuspended in 200 μl SDS lysis buffer (50 mM HEPES/NaOH pH 7.5, 1% SDS, 10 mM EDTA, 1 mM PMSF, and Roche ULTRA protease inhibitor cocktail (cat. 05892791001)) on ice for 10 min. Sonication was performed using Bioruptor Pico (Diagenode, cat. B01060010) on high setting for 30 s, followed by centrifugation of lysates to remove cellular debris. 100 μl of sheared chromatin from each tube was then diluted 10X, with 5% saved as Input DNA and the rest prepared for either PPARγ or RXR IP.

PPARγ WT, PPARγ KD, RXR, and Input libraries were prepared in duplicate from two independent biological replicates. For ChIP-seq, sequencing data was mapped to the human genome (GRCh38) using STAR [19] with parameters appropriate for ungapped alignments. Peaks were called for each sample with input samples as background by HOMER [20]. HOMER was also used for differential peak calling (PPARγ WT vs. KD and RXR WT vs. KD) and to annotate peaks to proximal genes as described in Ensembl v85 (http://www.ensembl.org/index.html). For bioinformatics analyses displayed in Figure 2C, F, 1031 "high-confidence sites" were defined by the following criteria: peak score $\geq$10 ($\geq$1 read per million), fold change (PPARγ WT vs. KD) $\geq$ 2, RXR peak called with strict overlap. Motif enrichment analysis was performed on this filtered peak list (1031 peaks) using HOMER against the standard list of known motifs; *de novo* motif discovery included consideration of lengths 8, 10, 12, 15,18 bp.

2.6. Annexin V-PI apoptosis assay

30,000 cells of each cell line were plated in triplicate on 6-well plates. Four days later, cells were prepared using the FITC—Annexin V, PI Kit (BD Biosciences, cat. 556547) according to the manufacturer's instructions. Flow cytometry was performed using the BD Accuri C6 instrument, with viable cells represented as the double-negative population.

2.7. 2D and 3D proliferation assays

For 2D proliferation assays, 30,000 cells of each cell line were plated in triplicate on 6-well plates. The following day (represented as Day 0), cells were trypsinized and counted using the Countess Automated Cell Counter (Invitrogen, cat. C10281), as per the manufacturer's instructions with Trypan blue. Cells were then counted again at the

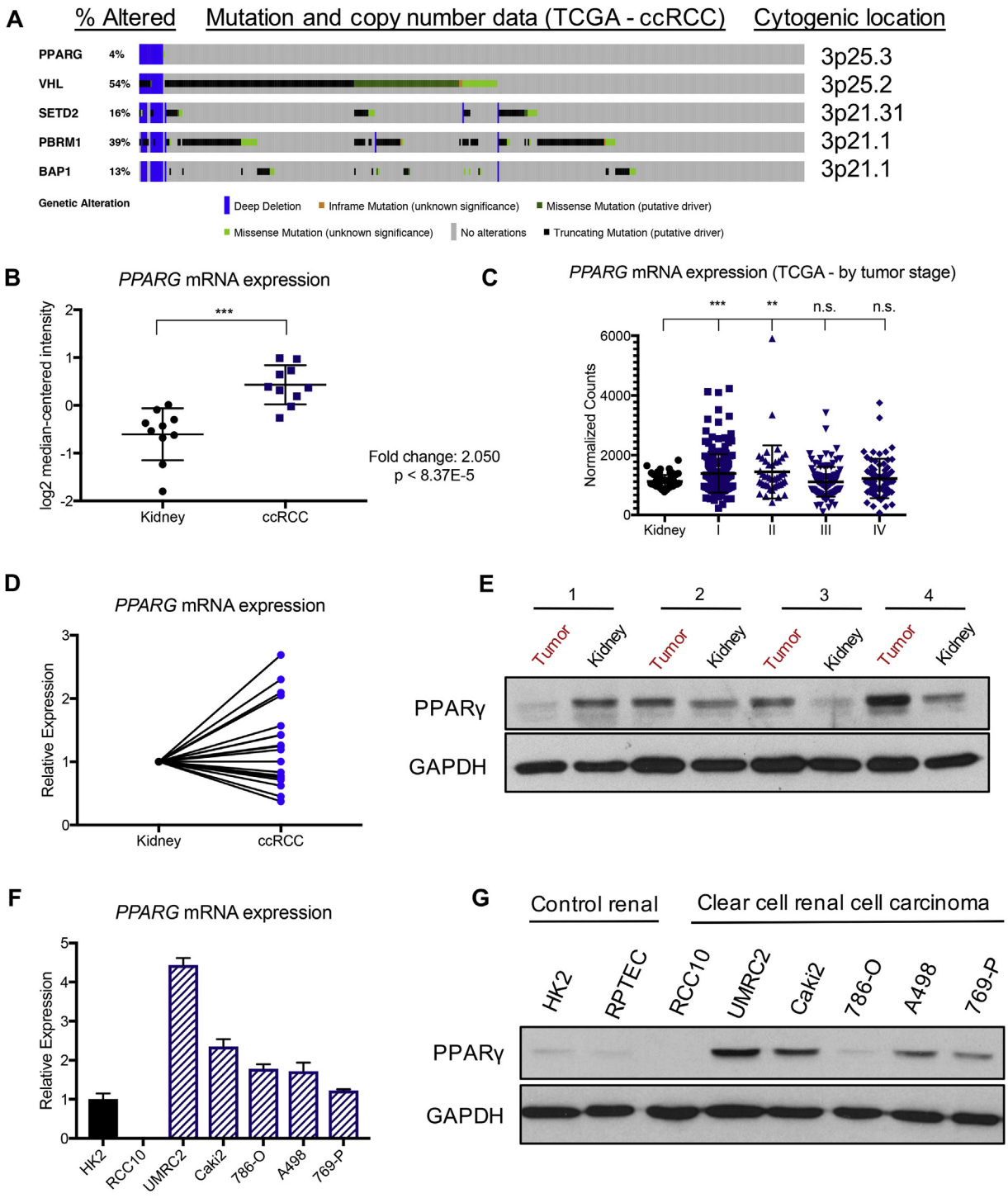

Figure 1: PPARγ expression in ccRCC patient samples and cell lines. A. Frequency of select chromosome 3p gene alterations in ccRCC tumors (cBioPortal). n = 448 patients. B. *PPARG* mRNA expression in ccRCC and adjacent healthy kidney tissue from Gumz Renal microarray dataset. *** ($p < 0.001$). C. *PPARG* mRNA expression in ccRCC and adjacent healthy kidney tissue from TCGA data set, stratified according to tumor stage. *** ($p < 0.001$), ** ($p < 0.01$), n.s. = not significant. D. RT-qPCR for *PPARG* expression in eighteen tumor-normal paired samples. E. Western blot for PPARγ expression in four tumor-normal paired samples. F. *PPARG* mRNA expression in control renal cell line (HK2, black bar) and ccRCC cell lines (RCC10 through 769-P, blue bars). G. PPARγ protein expression in control renal cell lines (HK2, RPTEC), ccRCC cell lines (RCC10 through 769-P).

indicated timepoints. For 3D proliferation assays, 3,000 cells of each cell line were plated in 24 wells of a Corning Costar 96-well Ultra-low attachment round bottom plate (Sigma–Aldrich, cat. CLS7007) [21]. Cells were mixed with Matrigel (BD Biosciences, cat. 356234) at a final concentration of 2.5%, and plates were centrifuged at 1800 rpm for 10 min to form spheroids. The following day (represented as Day 0), spheroids were imaged using the Invitrogen EVOS FL Auto Cell Imaging System and were imaged again, at the indicated timepoints, over the course of two weeks. Spheroid volume was calculated using a previously published ImageJ macro [22].

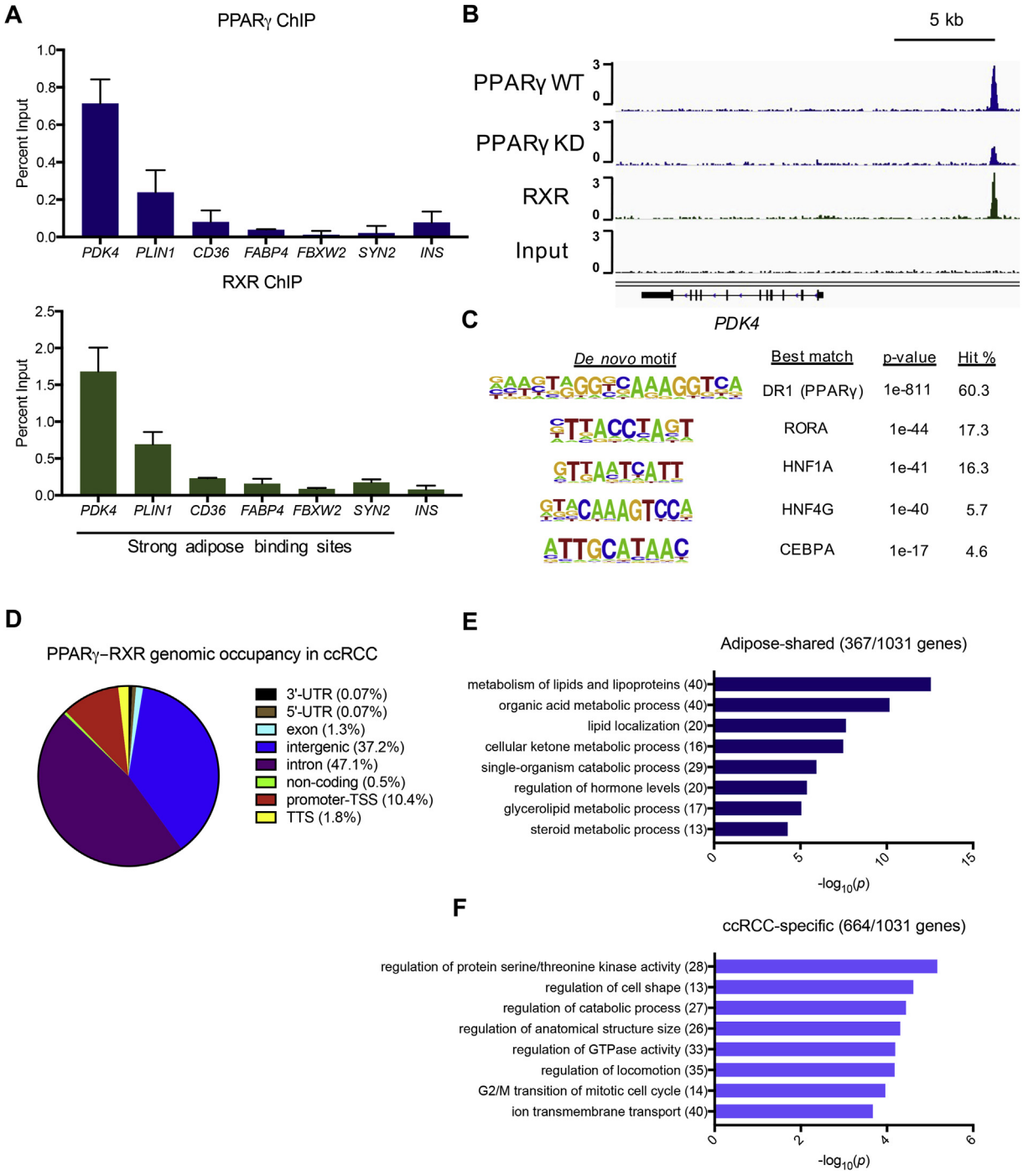

Figure 2: Genome-wide analysis of PPARγ-RXR binding in ccRCC. A. PPARγ and RXR enrichment at a subset of strong adipocyte binding sites in UMRC2 ccRCC cells (*INS*, negative control) assayed by ChIP-qPCR. B. ChIP-seq tracks of PPARγ WT, PPARγ KD, RXR and Input, showing binding to enhancer site −12 kb from *PDK4*. C. *De novo* motif analysis of PPARγ and RXR binding sites. For bioinformatics analyses displayed in C-F, 1031 "high-confidence sites" were defined by the following criteria: peak score ≥10 (≥1 read per million), fold change (WT vs. KD) ≥2, RXR peak called with strict overlap. D. Frequency of PPARγ-RXR heterodimer occupancy at various genomic locations, defined by HOMER annotate peaks. E. Gene ontology of PPARγ and RXR binding sites, annotated to nearest gene. 367/1031 genes (36%) were directly shared with human adipose. Data were compared to published PPARγ ChIP-seq from an adipocyte cell line [31]. Numbers in parenthesis indicate number of genes per category. F. Gene ontology of PPARγ and RXR binding sites, annotated to nearest gene. 664/1031 genes (64%) were unique to ccRCC. Data were compared to published PPARγ ChIP-seq from an adipocyte cell line [31]. Numbers in parenthesis indicate number of genes per category.

2.8. Subcutaneous xenograft

Experiments were approved by the Animal Care and Use Committee at the University of Pennsylvania. Six female NIH-III nude mice (Charles River Laboratories, 4–6 weeks old) were injected in each flank with 5×10^6 UMRC2 control or *PPARG* KO cells. Cells were resuspended in ice-cold PBS and were mixed 1:1 with Matrigel (BD Biosciences, cat. 356234) in a final volume of 200 μL per injection. Tumor volumes were recorded at the indicated timepoints using caliper measurements,

calculated by the formula $V = (\pi/6)\ (L)\ (W^2)$, where L was the longer measurement and W was the shorter measurement. At Day 75 post-injection, mice were sacrificed by CO_2 inhalation, and tumors were dissected for further analyses.

2.9. Immunohistochemistry

Xenograft tumors were dehydrated, embedded in paraffin, and sectioned for staining. Immunohistochemistry was performed as previously described [4] using 1:200 PPARγ (Cell Signaling Technology, cat. 2435), 1:100 Ki67 (Abcam, cat. Ab15580), and 1:400 Cleaved Caspase-3 (Cell Signaling Technology, cat. 9661).

2.10. Oil Red O staining

Oil Red O powder (350 mg) was dissolved in 100 mL 100% isopropanol as a stock solution. Working solutions were prepared by mixing 60% stock with 40% H_2O, vortexing, and resting for 30 min at room temperature before filtering through a 0.2 μm filter. Cells were washed twice in PBS, fixed in 4% paraformaldehyde for 15 min, and then incubated with the Oil Red O working solution for 30 min at room temperature. Three more PBS washes were performed before cells were counterstained with hematoxylin and coverslipped for imaging.

2.11. BODIPY (493/503) staining

50,000 cells of each cell line were plated in triplicate on 6-well plates. Three days later, live cells were washed twice in PBS and incubated in 2 μg/mL BODIPY 493/503 (Life Technologies, cat. D3922) in PBS for 15 min at 37 °C. After staining and trypsinization, cells were washed twice in PBS and fixed in 2% paraformaldehyde for 15 min in the dark. Fixed cells were washed and resuspended in PBS, passed through a cell strainer, and flow cytometry was performed on a BD Accuri C6 instrument under FL-1.

2.12. Triglyceride measurement

Xenograft tumors were homogenized in complete lysis buffer (50 mM Tris pH 7.4, 140 mM NaCl, 0.1% Triton X-100, 1 mM PMSF) containing Roche ULTRA protease inhibitor cocktail (cat. 05892791001) using a Tissue-Tearor (BioSpec Products, cat. 985370). Triglyceride content was measured using the LiquiColor Triglycerides kit (Stanbio Laboratory, cat. 2100) according to the manufacturer's instructions, and data were normalized to weight of each sample.

2.13. Statistics

Statistical analyses were performed using GraphPad Prism version 7 software, using unpaired t-test with Welch's correction. Data are presented as mean ± SEM of at least three independent experiments. Statistical significance was defined as *** ($p < 0.001$), ** ($p < 0.01$), * ($p < 0.05$), n.s. = not significant.

3. RESULTS

3.1. PPARγ expression in ccRCC patient samples and cell lines

A 43 megabase region of chromosome 3p harbors *bona fide* and putative tumor suppressor genes in ccRCC [23] including von Hippel-Lindau (*VHL*), the most commonly mutated gene in ccRCC and initiating tumorigenic event [24]. Unlike tumor suppressor genes located in this region, such as *VHL*, *SETD2*, *PBRM1,* and *BAP1*, *PPARG* is free from mutations which could render the protein non-functional or functional as a dominant-negative factor and retains wildtype sequence in 96% of ccRCC tumors (Figure 1A). *PPARG* mRNA expression is elevated in early-stage ccRCC relative to matched healthy kidney tissue (Figure 1B) [25,26]. The Cancer Genome Atlas (TCGA) RNA-seq data stratified according to tumor stage confirmed a significant increase in *PPARG* transcripts in stage I and II patients, with non-significant changes in stages III and IV relative to normal kidney tissue (Figure 1C). To verify *PPARG* mRNA and protein expression in ccRCC, we examined matched tumor/normal pairs by RT-qPCR and Western blot. *PPARG* mRNA (Figure 1D) and protein (Figure 1E) abundances were variable between tumor/normal samples, yet a subset of samples displayed elevated PPARγ expression relative to adjacent healthy kidney tissue. PPARγ expression in the kidney is highest in medullary collecting ducts [27,28] and is not expressed significantly in renal proximal tubule epithelial cells (RPTEC), a proposed cell-of-origin for ccRCC [29,30]. This may explain the heterogeneity observed across the kidney lysates sampled. We further examined PPARγ expression in a panel of ccRCC cell lines relative to immortalized (HK2) and purified primary (RPTEC) cells (Figure 1F, G) and found elevated mRNA and protein abundance in ccRCC relative to control in 4 out of 6 lines tested.

3.2. Genome-wide analysis of PPARγ-RXR binding in ccRCC

To understand the functional role of PPARγ in kidney cancer, we sought to characterize the PPARγ-RXR cistrome in the context of ccRCC and determine the relatedness of genomic occupancy to that found in adipocytes. ChIP-qPCR interrogating a number of adipocyte sites [31] in the UMRC2 cell line revealed coordinated occupancy for PPARγ and its heterodimeric binding partner RXR at *PDK4* and *PLIN1* (Figure 2A). To examine occupancy across the entire genome, we performed chromatin immunoprecipitation followed by deep sequencing (ChIP-seq) for PPARγ and RXR. We identified 1031 binding sites based on the following criteria: peak score greater than or equal to 10, wildtype vs. knockdown fold change greater than or equal to 2 (validation of PPARγ protein knockdown in Supplementary Fig. 1A), and RXR peak called with strict overlap (Figure 2B, Supplementary Table 1). We validated PPARγ binding at eight of the top sites called in our data set based on peak score using control and *PPARG* KO cells (Supplementary Figs. 2A–C). Additionally, we addressed the functionality of PPARγ binding in ccRCC cells through an shRNA-resistant cDNA rescue experiment. Ectopic expression of PPARγ increased the expression of *SLC38A4*, a gene with two PPARγ-RXR binding sites within 10 kb of the transcriptional start site (Supplementary Figs. 2D and 2E). When cells were treated with shRNA targeting *PPARG*, *SLC38A4* expression was diminished, but not when cells also contained the resistant cDNA (Supplementary Fig. 2F). These data suggest that *SLC38A4* is a direct transcriptional target of PPARγ in ccRCC and provide evidence that endogenous PPARγ activity regulates gene expression in our cell culture models.

Through *de novo* motif analysis, we found that the canonical nuclear receptor direct repeat 1 (DR1) motif is most highly enriched under PPARγ-RXR bound DNA in ccRCC, present at 60.3% of sites (Figure 2C). Other transcription factor motifs represented include RAR-related orphan receptor alpha (RORA) at 17.3% of sites and the hepatocyte nuclear factors alpha (HNF1A, 16.3% of sites) and gamma (HNF4G, 5.7% of sites). Interestingly, the C/EBP motif, which is found at 91% of PPARγ-binding regions in adipocytes [32], is only found at 4.6% of PPARγ-RXR-bound regions in ccRCC. Consistent with previously published ChIP-seq data sets in tissues including adipocytes and macrophages [33,34], PPARγ-RXR is bound most frequently at intergenic (37.2%) and intronic (47.1%) regions of the genome in ccRCC, rather than at promoter-transcriptional start sites (10.4%) (Figure 2D). We then annotated peaks to the nearest gene and performed gene ontology analysis to determine putative PPARγ-regulated pathways in ccRCC. Annotation of "adipose-shared" genes

include "metabolism of lipids and lipoproteins", "organic acid metabolic process", and "lipid localization" (Figure 2E), whereas "ccRCC-specific" genes belonged to cellular processes broadly important in cancer cell biology, including signal transduction and regulation of cell shape and size (Figure 2F).

3.3. PPARγ is dispensable for ccRCC viability and proliferation *in vitro*

As PPARγ was shown to bind near genes associated with regulation of protein serine/threonine kinase activity and G2/M transition of mitotic cell cycle in ccRCC (Figure 2F), we hypothesized that its loss would affect cell growth over time. Upon confirming effective knockout of PPARγ using CRISPR-Cas9 (Figure 3A, Supplementary Fig. 1B), we subjected UMRC2 and A498 ccRCC cell lines to a variety of *in vitro* assays to determine the functional consequence of PPARγ loss. *PPARG* KO did not affect the viability (Figure 3B, C) or proliferation rate (Figure 3D, E) of either cell line when cells were grown in replete conditions (21% O_2, 25 mM glucose and 10% FBS). Since oxygen and nutrient limitation can profoundly influence cancer cell growth, we embedded control and *PPARG* KO cells in Matrigel and allowed tumor spheroids to proliferate over the course of two weeks. *PPARG* KO did not affect spheroid volume during the assay (Figure 3F—H).

Additional "ccRCC-specific" PPARγ bound genes included those involved in "regulation of cell shape" and "regulation of locomotion", which we hypothesized could affect migratory capacity. We plated UMRC2 and A498 cells to confluency and performed an *in vitro* scratch assay to measure migration over the course of 16 h, a timepoint chosen based on the nearly complete recovery of the wound prior to the doubling time. We found no significant difference in the percentage of wound healing that occurred between control and *PPARG* KO cells (Supplementary Figs. 3A and 3B). We also found that PPARγ depletion only modestly affected anchorage-independent growth of UMRC2 and A498 ccRCC cells (Supplementary Figs. 3C and 3D).

3.4. PPARγ is dispensable for ccRCC xenograft tumor growth *in vivo*

To assess the function of PPARγ in ccRCC tumor growth *in vivo*, we implanted UMRC2 control and *PPARG* KO cells subcutaneously into opposing flanks of NIH-III nude mice. Analysis of tumor volume (Figure 4A) over the course of the experiment and tumor weights at day 75 post-injection (Figure 4B) revealed no significant difference in the growth of *PPARG* KO tumors relative to control. Additionally, control and *PPARG* KO tumors were sectioned and immunohistochemistry was performed for markers of proliferation (Ki67) and apoptosis (cleaved caspase-3), as well as to confirm PPARγ loss over the duration of the assay (Figure 4C). Quantitation of these markers revealed no significant difference between control and *PPARG* KO tumors, suggesting that PPARγ is dispensable for ccRCC cell growth *in vivo* (Figure 4D, E).

3.5. Lipid storage and triglyceride synthesis occur independently of PPARγ in ccRCC

As PPARγ is responsible for promoting lipid uptake and storage in adipocytes and is bound near lipid metabolism related genes in our model (Figure 2E), we hypothesized that its loss in ccRCC would reduce neutral lipid content. Surprisingly, we found that loss of PPARγ did not affect lipid accumulation in either ccRCC cell line tested *in vitro* by Oil Red O (Figure 5A) or BODIPY 493/503 (Figure 5B) staining. In agreement with this, expression of a number of proteins involved in *de novo* lipogenesis that are reduced following hepatocyte-specific deletion of PPARγ [11], including sterol regulatory element-binding protein 1 (SREBP1), fatty acid synthase (FASN), and stearoyl-CoA desaturase 1 (SCD), did not change substantially following PPARγ loss in our models (Figure 5C). Additionally, we measured triglyceride levels in control and *PPARG* KO xenograft tumors to determine whether exposure to oxygen and nutrient depletion *in vivo* would affect the ability of the cells to store triglyceride. Consistent with our *in vitro* results, we found no significant difference in triglyceride content between control and *PPARG* KO tumors (Figure 5D). These data indicate that PPARγ is dispensable for the "clear cell" phenotype of renal cancer with regard to triglyceride synthesis and storage.

4. DISCUSSION

"Druggability" of nuclear receptors via small molecule agonists or antagonists make them appealing therapeutic targets to treat diseases like diabetes and cancer. Across various tumor types, studies have revealed both oncogenic and tumor suppressive roles for PPARγ [35]. Heterozygous deletion of PPARγ in mice has demonstrated that it primarily acts as a tumor suppressor in chemically-induced models of colon [36], breast, ovarian and skin cancers [37], whereas newly uncovered oncogenic functions for PPARγ have been reported in bladder cancer using *in vitro* cell culture models [38,39]. We hypothesized that PPARγ would promote ccRCC tumorigenesis due to the fact that its lipid-laden phenotype is tightly linked to cell viability and proliferation. Our lab previously reported that suppression of the lipid droplet coat protein perilipin 2 in ccRCC reduces neutral lipid accumulation, engaging the endoplasmic reticulum stress response and causing tumor regression [4]. Additionally, cells defined by constitutive mTORC1 signaling such as ccRCC [16,40] require import of exogenous unsaturated fatty acids during hypoxia to maintain membrane homeostasis and prevent cell death [5,41]. However, our current understanding of the molecular mediators of lipid uptake and storage in ccRCC is limited.

In this study, we performed loss-of-function experiments to elucidate PPARγ's role in ccRCC in established cell lines both *in vitro* and *in vivo*. PPARγ deletion in two ccRCC cell lines affected neither viability, proliferation, migratory capacity *in vitro*, nor tumor growth in a subcutaneous xenograft model. Surprisingly, we also show that PPARγ is dispensable for lipid storage and maintenance of total triglyceride levels in ccRCC cells grown both *in vitro* and *in vivo*. While our data collectively suggest that PPARγ is not required for ccRCC progression, we cannot exclude a potential role for this nuclear receptor in tumor initiation. The stage-specific upregulation of *PPARG* transcripts in stage I and II kidney tumors (Figure 1B—C) is consistent with PPARγ protein expression patterns in human prostate cancer [42]. Functionally, this may reflect a role for PPARγ in epithelial-to-mesenchymal transition of renal epithelium to ccRCC, although this remains to be explored. *PPARG* expression may also be inversely related to the differentiation status of tumors, as previously reported in liposarcoma [43,44].

One factor that may influence PPARγ's function in regulating ccRCC gene expression is cooperative transcription factor binding. For example, CCAAT-enhancer-binding proteins (C/EBPs) have been shown to be required for robust PPARγ target gene expression in adipocytes [32], yet the C/EBP motif only appeared under ~5% of the binding sites called in ccRCC (Figure 2C). Lack of PPARγ/C/EBP cooperativity may underlie the lack of "classic" PPARγ target gene expression including *CD36*, *FABP4*, and other genes broadly important in lipid and glucose metabolism (Supplementary Fig. 1C) and demonstrate distinct PPARγ action in ccRCC vs. adipose tissue. Additionally, *de novo* motif analysis revealed that the retinoic acid

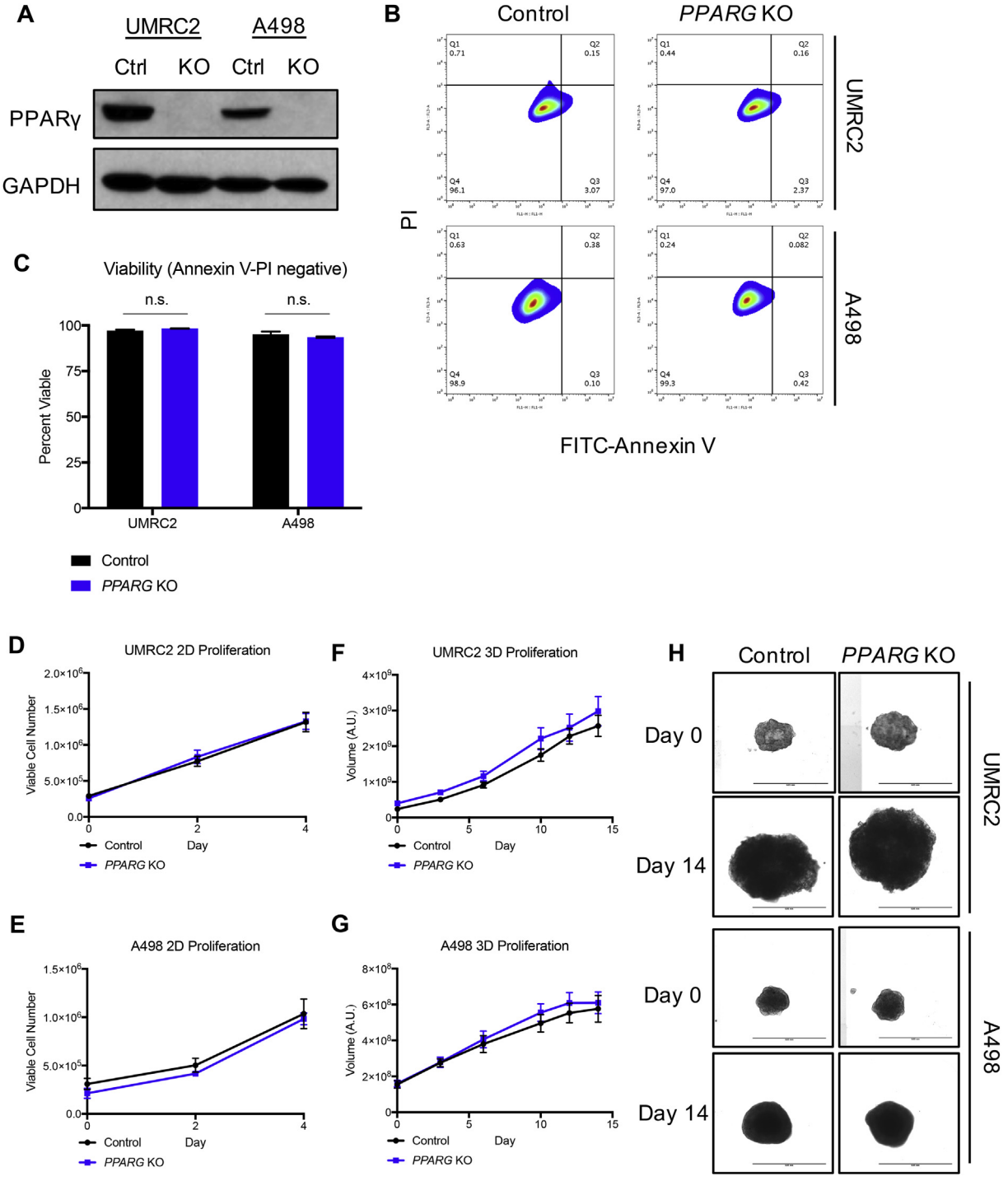

Figure 3: PPARγ is dispensable for ccRCC viability and proliferation *in vitro*. A. Western blot of PPARγ levels in UMRC2 and A498 cells following *PPARG* KO. B. Annexin V—PI flow cytometry plots for UMRC2 and A498 control and *PPARG* KO cells. C. Quantification of Annexin V—PI double-negative population (lower left quadrant) for UMRC2 and A498 control and *PPARG* KO cells. D. Growth curve of UMRC2 cell line measuring proliferation rate of control and *PPARG* KO cells over the course of four days. E. Growth curve of A498 cell line measuring proliferation rate of control and *PPARG* KO cells over the course of four days. F. Growth curve of UMRC2 tumor spheroids measuring proliferation rate of control and *PPARG* KO cells over the course of two weeks. G. Growth curve of A498 tumor spheroids measuring proliferation rate of control and *PPARG* KO cells over the course of two weeks. H. Representative images of UMRC2 and A498 control and *PPARG* KO tumor spheroids at indicated timepoints. Scale bar = 100 μm.

receptor-related orphan receptor alpha (RORα) motif is the second most commonly enriched motif under PPARγ-RXR-bound DNA in ccRCC (Figure 2C). A recent report demonstrated that RORα reduces PPARγ transcriptional activity via the recruitment of histone deacetylase 3 to PPARγ target gene promoters in the livers of mice fed HFD [45]. PPARγ-RORα co-localization in ccRCC and negative regulation of lipid metabolism-related genes would be consistent with the phenotypes observed in our experiments, as PPARγ depletion did not reduce triglyceride content or significantly alter expression of *de novo* lipogenesis enzymes (Figure 5).

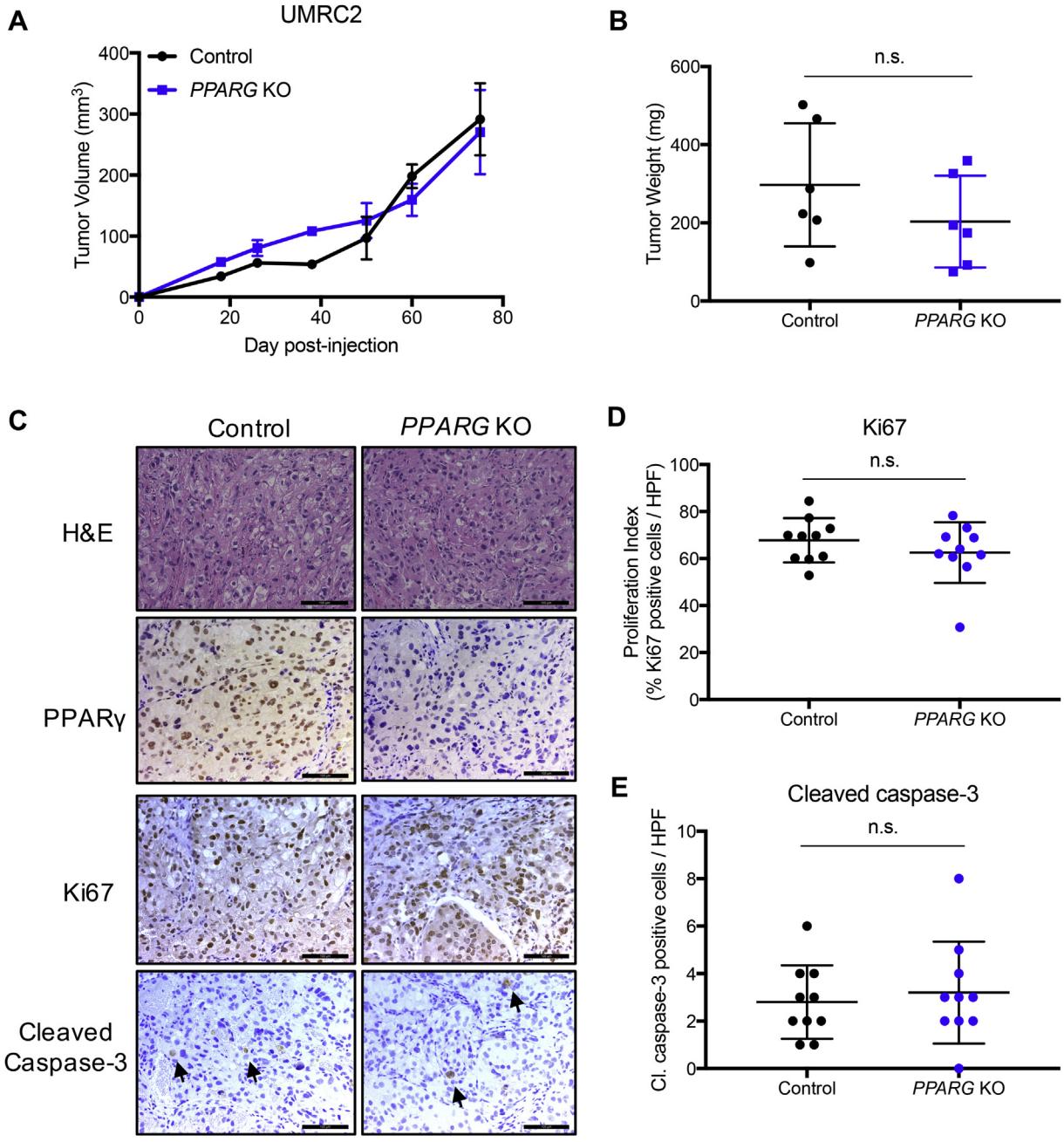

Figure 4: PPARγ is dispensable for ccRCC xenograft tumor growth *in vivo.* A. Tumor volume measurements for UMRC2 control and *PPARG* KO subcutaneous xenografts at indicated timepoints. B. Tumor weight measurements for UMRC2 control and *PPARG* KO subcutaneous xenografts at day 75 post-injection. n.s. = not significant. C. Representative images of hematoxylin and eosin (H&E) staining and PPARγ, Ki67 and cleaved caspase-3 immunohistochemistry from UMRC2 control and *PPARG* KO subcutaneous xenograft tumors. Scale bar = 100 μm. D. Quantification of Ki67-positivity shown in Figure 4C. n.s. = not significant. E. Quantification of cleaved caspase-3-positivity shown in Figure 4C. n.s. = not significant.

We considered that compensatory up-regulation of other PPAR family members may underlie the lack of phenotypes observed in our experiments; however, we determined that *PPARG* KO cells do not increase expression of *PPARA* or *PPARD* (Supplementary Fig. 1D). Indeed, expression of *PPARA, PPARGC1A,* and additional genes involved in beta-oxidation of lipids are highly suppressed in ccRCC relative to healthy renal tubule epithelium [46]. Ectopic expression of such factors in ccRCC reduces tumor growth [47], further illustrating the importance of reprogramming lipid metabolism from an oxidative to anabolic state in this tumor type. In conclusion, our investigation of PPARγ in ccRCC led to a novel PPARγ-RXR cistrome, which shares both similarities and differences with published cistromes in tissues such as adipocytes and macrophages. Of note, our dataset will be beneficial to researchers studying cell type-specific functions of PPARγ in cancer as well as the role of other subfamily 1 nuclear receptors that heterodimerize with RXR in ccRCC. Finally, while PPARγ is expressed in ccRCC tumors, it does not appear to be necessary for tumor maintenance based on our assays.

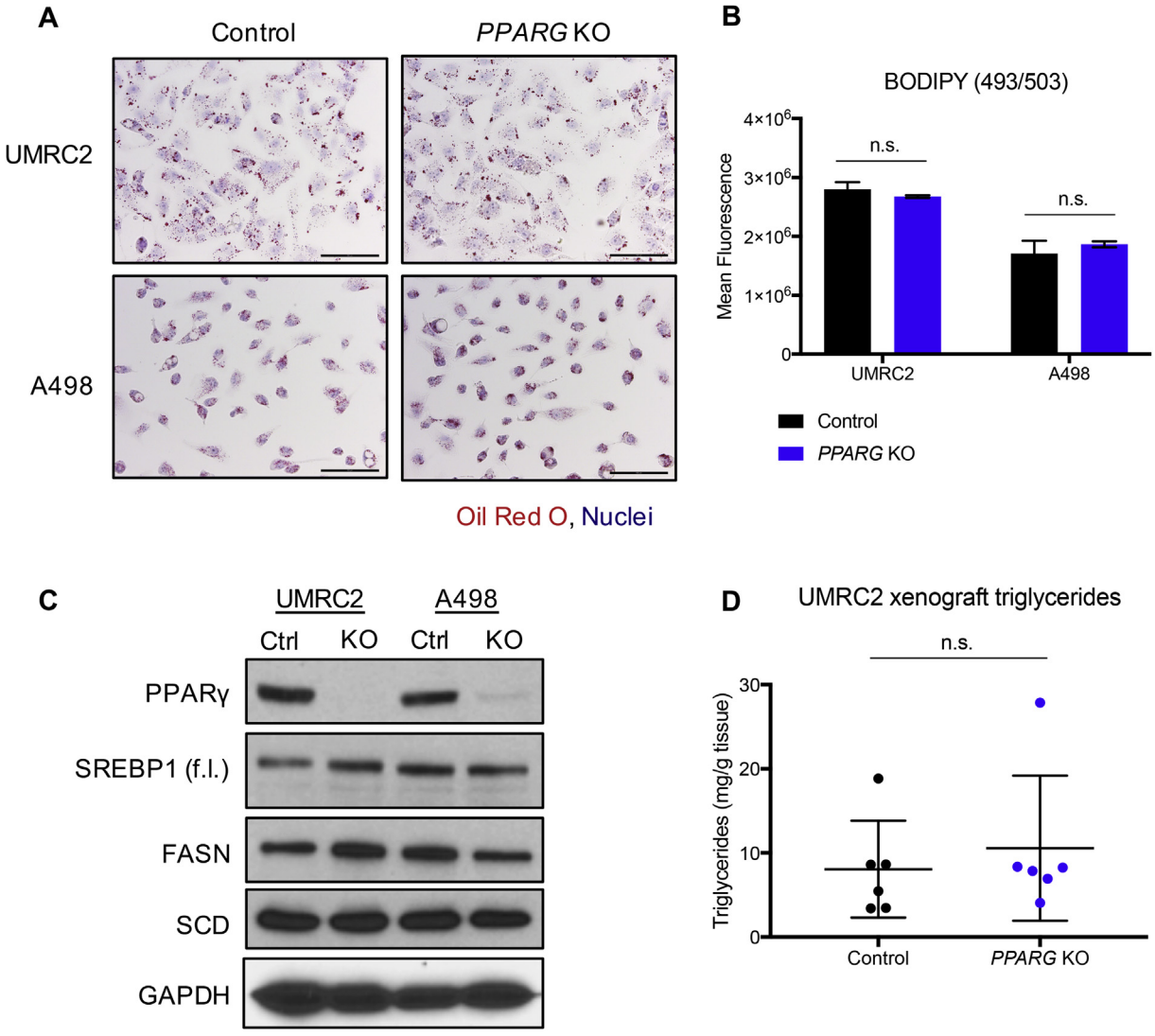

Figure 5: Lipid storage and triglyceride synthesis occur independently of PPARγ in ccRCC. A. Representative images of UMRC2 and A498 control and *PPARG* KO cells stained with Oil Red O and counterstained with hematoxylin to visualize nuclei. Scale bar = 100 μm. B. Quantification of BODIPY (493/503) staining of UMRC2 and A498 control and *PPARG* KO cell lines. n.s. = not significant. C. Western blot of PPARγ, SREBP1 (f.l. = full length), FASN, and SCD in UMRC2 and A498 control and *PPARG* KO cell lines. D. Triglyceride content of UMRC2 control and *PPARG* KO subcutaneous xenograft tumors. n.s. = not significant.

AUTHORS' CONTRIBUTIONS

D.J.S.[1,4] and M.C.S. designed the study, D.J.S.[3] provided technical support for ChIP and ChIP-seq experiments. D.J.S.[1,4], N.S., and A.B. performed experiments and analyzed data. D.J.S.[1,4] and M.C.S. wrote the manuscript.

ACKNOWLEDGMENTS

We thank John Tobias for bioinformatics assistance, Raymond Soccio for guidance with ChIP experiments, and Jeff Ishibashi for technical assistance. We also thank Karin Eisinger and Mitch Lazar for their critical comments on the manuscript. This work was supported by grants T32 HD083185 and F31 CA206381 (to D.J.S.1,4), R01 DK098542 (to D.J.S.3), and P01 CA104838 to M.C.S.

CONFLICTS OF INTEREST

None declared.

APPENDIX A. SUPPLEMENTARY DATA

Supplementary data related to this article can be found at https://doi.org/10.1016/j.molmet.2018.05.013.

REFERENCES

[1] N.C. Institute, 2018. SEER cancer stat facts: kidney and renal pelvis cancer.
[2] Rydzanicz, M., Wrzesiński, T., Bluyssen, H.A., Wesoły, J., 2013. Genomics and epigenomics of clear cell renal cell carcinoma: recent developments and potential applications. Cancer Letters 341:111–126.
[3] Wettersten, H.I., Aboud, O.A., Lara Jr., P.N., Weiss, R.H., 2017. Metabolic reprogramming in clear cell renal cell carcinoma. Nature Reviews Nephrology 13:410.
[4] Qiu, B., Ackerman, D., Sanchez, D.J., Li, B., Ochocki, J.D., Grazioli, A., et al., 2015. HIF2α-dependent lipid storage promotes endoplasmic reticulum homeostasis in clear-cell renal cell carcinoma. Cancer Discovery 5:652–667.

[5] Young, R.M., Ackerman, D., Quinn, Z.L., Mancuso, A., Gruber, M., Liu, L., et al., 2013. Dysregulated mTORC1 renders cells critically dependent on desaturated lipids for survival under tumor-like stress. Genes & Development 27:1115—1131.

[6] Ahmadian, M., Suh, J.M., Hah, N., Liddle, C., Atkins, A.R., Downes, M., et al., 2013. PPARγ signaling and metabolism: the good, the bad and the future. Nature Medicine 19:557.

[7] Tontonoz, P., Hu, E., Spiegelman, B.M., 1994. Stimulation of adipogenesis in fibroblasts by PPARγ2, a lipid-activated transcription factor. Cell 79:1147—1156.

[8] Wang, F., Mullican, S.E., DiSpirito, J.R., Peed, L.C., Lazar, M.A., 2013. Lipoatrophy and severe metabolic disturbance in mice with fat-specific deletion of PPARγ. Proceedings of the National Academy of Sciences 110: 18656—18661.

[9] Krishnan, J., Suter, M., Windak, R., Krebs, T., Felley, A., Montessuit, C., et al., 2009. Activation of a HIF1α-PPARγ axis underlies the integration of glycolytic and lipid anabolic pathways in pathologic cardiac hypertrophy. Cell Metabolism 9:512—524.

[10] Chawla, A., Barak, Y., Nagy, L., Liao, D., Tontonoz, P., Evans, R.M., 2001. PPAR-γ dependent and independent effects on macrophage-gene expression in lipid metabolism and inflammation. Nature Medicine 7:48.

[11] Morán-Salvador, E., López-Parra, M., García-Alonso, V., Titos, E., Martínez-Clemente, M., González-Périz, A., et al., 2011. Role for PPARγ in obesity-induced hepatic steatosis as determined by hepatocyte-and macrophage-specific conditional knockouts. The FASEB Journal 25:2538—2550.

[12] Collet, N., Théoleyre, S., Rageul, J., Mottier, S., Jouan, F., Rioux-Leclercq, N., et al., 2011. PPARγ is functionally expressed in clear cell renal cell carcinoma. International Journal of Oncology 38:851—857.

[13] Zhu, C., Wei, J., Tian, X., Li, Y., Li, X., 2015. Prognostic role of PPAR-γ and PTEN in the renal cell carcinoma. International Journal of Clinical and Experimental Pathology 8:12668.

[14] Fujita, M., Yagami, T., Fujio, M., Tohji, C., Takase, K., Yamamoto, Y., et al., 2011. Cytotoxicity of troglitazone through PPARγ-independent pathway and p38 MAPK pathway in renal cell carcinoma. Cancer Letters 312:219—227.

[15] Shiau, C.-W., Yang, C.-C., Kulp, S.K., Chen, K.-F., Chen, C.-S., Huang, J.-W., et al., 2005. Thiazolidenediones mediate apoptosis in prostate cancer cells in part through inhibition of Bcl-xL/Bcl-2 functions independently of PPARγ. Cancer Research 65:1561—1569.

[16] C.G.A.R. Network, 2013. Comprehensive molecular characterization of clear cell renal cell carcinoma. Nature 499:43.

[17] Sanjana, N.E., Shalem, O., Zhang, F., 2014. Improved vectors and genome-wide libraries for CRISPR screening. Nature Methods 11:783.

[18] Wiederschain, D., Susan, W., Chen, L., Loo, A., Yang, G., Huang, A., et al., 2009. Single-vector inducible lentiviral RNAi system for oncology target validation. Cell Cycle 8:498—504.

[19] Dobin, A., Davis, C.A., Schlesinger, F., Drenkow, J., Zaleski, C., Jha, S., et al., 2013. STAR: ultrafast universal RNA-seq aligner. Bioinformatics 29:15—21.

[20] Heinz, S., Benner, C., Spann, N., Bertolino, E., Lin, Y.C., Laslo, P., et al., 2010. Simple combinations of lineage-determining transcription factors prime cis-regulatory elements required for macrophage and B cell identities. Molecular Cell 38:576—589.

[21] Vinci, M., Gowan, S., Boxall, F., Patterson, L., Zimmermann, M., Lomas, C., et al., 2012. Advances in establishment and analysis of three-dimensional tumor spheroid-based functional assays for target validation and drug evaluation. BMC Biology 10:29.

[22] Ivanov, D.P., Parker, T.L., Walker, D.A., Alexander, C., Ashford, M.B., Gellert, P.R., et al., 2014. Multiplexing spheroid volume, resazurin and acid phosphatase viability assays for high-throughput screening of tumour spheroids and stem cell neurospheres. PLoS One 9 e103817.

[23] Peña-Llopis, S., Christie, A., Xie, X.-J., Brugarolas, J., 2013. Cooperation and antagonism among cancer genes: the renal cancer paradigm. Cancer Research 73:4173—4179.

[24] Mandriota, S.J., Turner, K.J., Davies, D.R., Murray, P.G., Morgan, N.V., Sowter, H.M., et al., 2002. HIF activation identifies early lesions in VHL kidneys: evidence for site-specific tumor suppressor function in the nephron. Cancer Cell 1:459—468.

[25] Gumz, M.L., Zou, H., Kreinest, P.A., Childs, A.C., Belmonte, L.S., LeGrand, S.N., et al., 2007. Secreted frizzled-related protein 1 loss contributes to tumor phenotype of clear cell renal cell carcinoma. Clinical Cancer Research 13:4740—4749.

[26] Tun, H.W., Marlow, L.A., Von Roemeling, C.A., Cooper, S.J., Kreinest, P., Wu, K., et al., 2010. Pathway signature and cellular differentiation in clear cell renal cell carcinoma. PLoS One 5:e10696.

[27] Guan, Y., Zhang, Y., Davis, L., Breyer, M.D., 1997. Expression of peroxisome proliferator-activated receptors in urinary tract of rabbits and humans. American Journal of Physiology — Renal Physiology 273:F1013—F1022.

[28] Guan, Y., Hao, C., Cha, D.R., Rao, R., Lu, W., Kohan, D.E., et al., 2005. Thiazolidinediones expand body fluid volume through PPARγ stimulation of ENaC-mediated renal salt absorption. Nature Medicine 11:861.

[29] Yoshida, S., Imam, A., Olson, C., Taylor, C., 1986. Proximal renal tubular surface membrane antigens identified in primary and metastatic renal cell carcinomas. Archives of Pathology & Laboratory Medicine 110:825—832.

[30] Chen, F., Zhang, Y., Şenbabaoğlu, Y., Ciriello, G., Yang, L., Reznik, E., et al., 2016. Multilevel genomics-based taxonomy of renal cell carcinoma. Cell Reports 14:2476—2489.

[31] Soccio, R.E., Tuteja, G., Everett, L.J., Li, Z., Lazar, M.A., Kaestner, K.H., 2011. Species-specific strategies underlying conserved functions of metabolic transcription factors. Molecular Endocrinology 25:694—706.

[32] Lefterova, M.I., Zhang, Y., Steger, D.J., Schupp, M., Schug, J., Cristancho, A., et al., 2008. PPARγ and C/EBP factors orchestrate adipocyte biology via adjacent binding on a genome-wide scale. Genes & Development 22:2941—2952.

[33] Lefterova, M.I., Steger, D.J., Zhuo, D., Qatanani, M., Mullican, S.E., Tuteja, G., et al., 2010. Cell-specific determinants of peroxisome proliferator-activated receptor γ function in adipocytes and macrophages. Molecular and Cellular Biology 30:2078—2089.

[34] Schmidt, S.F., Jørgensen, M., Chen, Y., Nielsen, R., Sandelin, A., Mandrup, S., 2011. Cross species comparison of C/EBPα and PPARγ profiles in mouse and human adipocytes reveals interdependent retention of binding sites. BMC Genomics 12:152.

[35] Tontonoz, P., Spiegelman, B.M., 2008. Fat and beyond: the diverse biology of PPARγ. Annual Review of Biochemistry 77:289—312.

[36] Girnun, G.D., Smith, W.M., Drori, S., Sarraf, P., Mueller, E., Eng, C., et al., 2002. APC-dependent suppression of colon carcinogenesis by PPARγ. Proceedings of the National Academy of Sciences 99:13771—13776.

[37] Nicol, C.J., Yoon, M., Ward, J.M., Yamashita, M., Fukamachi, K., Peters, J.M., et al., 2004. PPARγ influences susceptibility to DMBA-induced mammary, ovarian and skin carcinogenesis. Carcinogenesis 25:1747—1755.

[38] Goldstein, J.T., Berger, A.C., Shih, J., Duke, F.F., Furst, L., Kwiatkowski, D.J., et al., 2017. Genomic activation of PPARG reveals a candidate therapeutic axis in bladder cancer. Cancer Research canres. 1701.2017.

[39] Halstead, A.M., Kapadia, C.D., Bolzenius, J., Chu, C.E., Schriefer, A., Wartman, L.D., et al., 2017. Bladder-cancer-associated mutations in RXRA activate peroxisome proliferator-activated receptors to drive urothelial proliferation. eLife 6.

[40] Turajlic, S., Larkin, J., Swanton, C., 2015. SnapShot: renal cell carcinoma. Cell 163, 1556—1556. e1551.

[41] Kamphorst, J.J., Cross, J.R., Fan, J., de Stanchina, E., Mathew, R., White, E.P., et al., 2013. Hypoxic and Ras-transformed cells support growth by scavenging unsaturated fatty acids from lysophospholipids. Proceedings of the National Academy of Sciences 110:8882—8887.

[42] Nakamura, Y., Suzuki, T., Sugawara, A., Arai, Y., Sasano, H., 2009. Peroxisome proliferator-activated receptor gamma in human prostate carcinoma. Pathology International 59:288—293.

[43] Tontonoz, P., Singer, S., Forman, B.M., Sarraf, P., Fletcher, J.A., Fletcher, C.D., et al., 1997. Terminal differentiation of human liposarcoma cells induced by ligands for peroxisome proliferator-activated receptor γ and the retinoid X receptor. Proceedings of the National Academy of Sciences 94:237–241.

[44] Demetri, G.D., Fletcher, C.D., Mueller, E., Sarraf, P., Naujoks, R., Campbell, N., et al., 1999. Induction of solid tumor differentiation by the peroxisome proliferator-activated receptor-γ ligand troglitazone in patients with liposarcoma. Proceedings of the National Academy of Sciences 96: 3951–3956.

[45] Kim, K., Boo, K., Yu, Y.S., Oh, S.K., Kim, H., Jeon, Y., et al., 2017. RORα controls hepatic lipid homeostasis via negative regulation of PPARγ transcriptional network. Nature Communications 8:162.

[46] Kang, H.M., Ahn, S.H., Choi, P., Ko, Y.-A., Han, S.H., Chinga, F., et al., 2015. Defective fatty acid oxidation in renal tubular epithelial cells has a key role in kidney fibrosis development. Nature Medicine 21:37.

[47] LaGory, E.L., Wu, C., Taniguchi, C.M., Ding, C.-K.C., Chi, J.-T., von Eyben, R., et al., 2015. Suppression of PGC-1α is critical for reprogramming oxidative metabolism in renal cell carcinoma. Cell Reports 12:116–127.

